Group refractive index reconstruction with broadband interferometric confocal microscopy

Daniel L. Marks,[1] Simon C. Schlachter,[1] Adam M. Zysk,[1,2] and Stephen A. Boppart[1,*]

[1]*Beckman Institute of Science and Technology, Department of Electrical and Computer Engineering, University of Illinois at Urbana-Champaign, 405 North Mathews Avenue, Urbana, Illinois 61801, USA*

[2]*Current address: Medical Imaging Research Center, Electrical and Computer Engineering Department, Illinois Institute of Technology, 3301 South Dearborn Street, Chicago, Illinois 60616, USA*

[*]*Corresponding author: boppart@uiuc.edu*

Received September 28, 2007; accepted December 16, 2007;
posted February 19, 2008 (Doc. ID 88016); published April 25, 2008

We propose a novel method of measuring the group refractive index of biological tissues at the micrometer scale. The technique utilizes a broadband confocal microscope embedded into a Mach–Zehnder interferometer, with which spectral interferograms are measured as the sample is translated through the focus of the beam. The method does not require phase unwrapping and is insensitive to vibrations in the sample and reference arms. High measurement stability is achieved because a single spectral interferogram contains all the information necessary to compute the optical path delay of the beam transmitted through the sample. Included are a physical framework defining the forward problem, linear solutions to the inverse problem, and simulated images of biologically relevant phantoms. © 2008 Optical Society of America

OCIS codes: 100.3010, 170.1790, 180.6900, 100.3190.

1. INTRODUCTION

Optical refractive index is a fundamental material property for which many measurement instruments exist. However, few instruments are able to probe the group refractive index of media at the micrometer scale. Recent work [1] has indicated that the group refractive index has potential diagnostic capability to distinguish breast cancer from normal tissues. To be able to further investigate the origin of the group refractive index contrast at the scale of organelles, we propose a new instrument. This instrument combines confocal microscopy with spectral interferometry [2] so that the group delay at each point in the medium can be precisely measured. Because spectral inteferometry measures the relative phase between frequencies in a single interferogram snapshot, the design is far less susceptible to vibrations and source intensity noise, and it does not require phase unwrapping. In this work, the 3-D transfer function of the microscope and linear solutions to the inverse problem for refractive index are derived, and a simulation is performed to demonstrate refractive index reconstruction on a cellular phantom.

The spatial refractive index distribution determines the behavior of many optical phenomena, including scattering processes and light-induced surface forces, which in turn are relevant to an array of optical sensing, imaging, and manipulation techniques [3]. For example, scattering processes arising from cellular and subcellular refractive index discontinuities are key to diagnostic techniques like diffuse optical tomography and optical coherence tomography [4,5]. The refractive index properties of cellular structures remains poorly understood, primarily due to the difficulty of direct measurement *in situ*. A more complete understanding of these properties would likely lead to improved diagnostic capabilities among various clinical optical imaging modalities.

Refractive index is an interesting diagnostic indicator in its own right. In addition to materials applications such as polymer composition measurement [6], crystal growth evaluation [7], and optical fiber assessment [8], a number of biomedical properties are observable based on refractive index changes. Recent studies have shown, for example, that refractive index variations hold significance for breast cancer evaluation [1]. Since the breast is comprised primarily of fat tissue, which has an elevated refractive index due to its high lipid concentration, the functional epithelial structures, having a much lower refractive index, are easily identified by direct measurement. Studies have also emphasized the importance of refractive index variations due to changes in biochemical environments. For instance, it has recently been shown that oxygen saturation modulates the refractive index of hemoglobin, thus affecting the optical measurement of blood oxygenation [9], a common medical practice.

A number of tomographic approaches have been developed for nondestructive imaging of subsurface optical refractive index distribution. These techniques often employ interferometric detection in order to exploit the highly sensitive optical pathlength measurements afforded by these techniques [10]. Projected index computed tomography (PICT), for example, uses a Michelson-type interferometer to measure the optical pathlength through an object over a fixed physical distance [11]. These data, when acquired at multiple lateral and rotational positions, can be used to reconstruct the spatial refractive index distribution using standard computed tomography

techniques. This technique is limited by the requirement that a reflective surface be placed behind the sample, which significantly constrains sample size. Bifocal optical coherence refractometry (BOCR) is another interferometric refractive index technique [12,13]. BOCR employs a Michelson-type interferometer with a pair of foci that are scanned depthwise through a sample. By measuring the distance between the two backscattering responses within the sample, a tomographic mapping of the refractive index distribution can be formed. This technique requires relatively uniform sample scattering but can be applied for *in vivo* imaging. A recent method, tomographic phase microscopy [14], measures the transmitted phase of monochromatic light through a thin sample to infer the refractive index using the inverse Radon transform. This method as implemented does not account for phase wrapping or the diffraction of the field; however, the methods of Fourier diffraction tomography could be applied to the instrument. A method of measuring refractive index by confocal microscopy uses the difference between the nominal focus position and the actual focus position induced by index of refraction variation [15]. Another similar method illuminates the sample with two confocal objectives to provide two reflectance maxima that are used to estimate refractive index and sample thickness [16].

The previous methods rely on measuring the backscattered light, delayed and refracted by the index of refraction variations. Instead of relying on backscattered signal, we devise a method of determining the refractive index from direct measurements of the group delay of the light transmitted through the sample. Analyzing the perturbation expansion [17,18] of the eikonal of a wavefront as a function of the refractive index, we find that the changes in ray travel time that are first order in the index perturbation are not affected by peturbations in the ray positions. This is a consequence of Fermat's principle and is the basis of travel time tomography and PICT. Because one expects to measure very small amounts of optical path delay variation when passing a ray through individual cellular organelles (10–200 nm additional path delay), a method that is insensitive to refraction of the ray path is warranted even if the apparatus is somewhat more complicated than a conventional confocal microscope.

In confocal microscopy, high numerical aperture (high-NA) focusing is typically used. Rather than being regarded as a single ray, the illumination beam is a converging cone of rays. Therefore, a new solution for travel-time tomography for high-NA illumination must be derived that does not assume that the illumination is a pencil beam. This paper derives such a framework and proposes an instrument for measuring the group refractive index of a medium. The instrument presented here is a transmission confocal microscope embedded in a Mach–Zehnder interferometer with spectral interferometric detection. The instrument does not require sample rotation or reference reflectors. The physical apparatus is suitable for integration with high-NA confocal microscope systems. The data acquisition is robust because it requires only that spectral interferograms be acquired as the sample is translated in three dimensions. Because the instrument acquires all the data needed at a given sample position in a single spectral interferogram snapshot, the method is insensitive to vibrations and source intensity noise. The instrument measures the complex group refractive index, which includes both a real component indicating the retardance at a given sample location and an imaginary part indicating the absorption.

2. DERIVATION OF REFRACTIVE INDEX RECONSTRUCTION RELATION

The proposed instrument is detailed in Fig. 1. The design is a transmission confocal microscope embedded in one arm of a Mach–Zehnder interferometer. Incident on the interferometer is a broadband source of illumination, e.g., a mode-locked laser or a superluminescent diode. Monochromatic illumination is not sufficient to infer the group refractive index, which inherently involves the propagation of polychromatic light. This illumination is divided by a beam splitter into a reference beam and a sample beam. The sample beam is focused by an illumination micro-

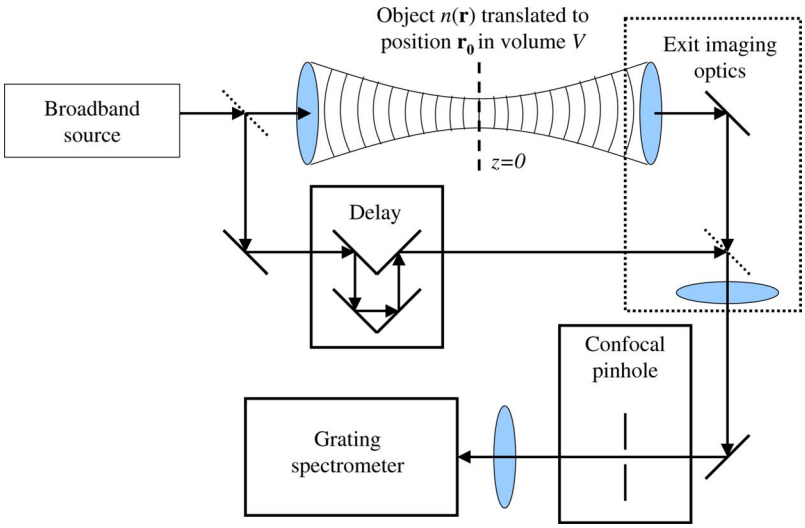

Fig. 1. (Color online) Diagram of group refractive index confocal microscopy instrument.

scope objective into the object space V. A second objective, confocal with the first, collects the illumination beam and recollimates it. The reference beam is adjusted so that the total delay through the reference arm is slightly less than that through the sample arm. The second beam splitter recombines the sample and reference beams, and the two beams are focused into a confocal pinhole. The beam is recollimated from this pinhole, and the spectrum of the field passing through the pinhole is sampled by spectral interference [2]. The data acquisition consists of translating the sample in three dimensions and acquiring the spectral interferograms.

The derivation consists of three sections. In Section 2, the field at the pinhole is computed for a single-frequency focused illumination beam scattered from the sample. This field is used to find the relationship between the 3-D Fourier components of the object refractive index at a single illumination frequency and the measured field at the pinhole. In Section 3, this relationship is extended to multiple illumination frequencies, thus allowing the group refractive index to be computed. In Section 4, a solution is found to the inverse scattering problem of inferring the group refractive index from the spectral interferogram measurements.

To find the field scattered to the pinhole by the sample, we consider the field $u(\mathbf{r})$ in the object space V. The field satisfies the inhomogeneous reduced wave equation:

$$\nabla^2 u(\mathbf{r}) + k^2[n_0(\mathbf{r}) + \epsilon n(\mathbf{r}-\mathbf{r_0})]^2 u(\mathbf{r}) = 0, \tag{1}$$

where k is the free-space wavenumber of the field, $n_0(\mathbf{r})$ is the refractive index representing the optical system of Fig. 1 without an object, and $n(\mathbf{r})$ is the inhomogeneneous refractive index of the object, which is treated as a perturbation on the order of a small parameter ϵ. The inhomogeneity $n(\mathbf{r})$ is zero outside of the volume V. We make the first Rytov approximation [19,20] where the field $u(\mathbf{r}) = u_0(\mathbf{r})\exp[\epsilon\phi(\mathbf{r})]$, where $u_0(\mathbf{r})$ obeys the unperturbed wave equation $\nabla^2 u_0 + k^2 n_0^2 u_0 = 0$ and ϕ is a complex phase. To first order in ϵ, the solution for ϕ is

$$u_0(\mathbf{r};k)\phi(\mathbf{r},\mathbf{r_0};k) = -2k^2 \int_V \mathrm{d}^3 r'\, g(\mathbf{r},\mathbf{r}';k) u_0(\mathbf{r}';k) n_0(\mathbf{r}') \times n(\mathbf{r}'-\mathbf{r_0}), \tag{2}$$

where $g(\mathbf{r},\mathbf{r}';k)$ is the Green's function that is the solution to the unperturbed wave equation $\nabla^2 g + k^2 n_0^2 g = -4\pi\delta(\mathbf{r}'-\mathbf{r})$. In the absence of an object, the refractive index in the volume V is $n_0(\mathbf{r};k) = n_b$. The illumination beam in V has a field denoted by $u_0(\mathbf{r};k)$. The field is given in terms of its Fourier spectrum at the beam waist plane $z = 0$:

$$u_0(\mathbf{r}';k) = (2\pi)^{-2} k^{-2} \int \mathrm{d}^2 q'\, \exp[i(\mathbf{q}'\cdot\mathbf{r}' + k_z(\mathbf{q}')z')]\tilde{B}\left(\frac{\mathbf{q}'}{k}\right), \tag{3}$$

where $\tilde{B}(\mathbf{q}'/k)$ is the Fourier expansion of the beam field in the plane $z = 0$, and $k_z(\mathbf{q}') = \sqrt{k^2 n_b^2 - q'^2}$. The scaling and normalization with k ensures that the beam amplitude at the focus is the same for all frequencies k. For a Gaussian beam, $\tilde{B}(\mathbf{q}'/k) = B_0 \exp(-q'^2\alpha^2/2k^2)$, where $\alpha = \pi/NA$, and NA is the numerical aperture of the focusing of the lens.

Next, we determine the Green's function $g(\mathbf{r},\mathbf{r}';k)$. In the volume V, the field is relayed to the pinhole plane P by the "exit imaging optics" shown in Fig. 1. These optics are composed of the lens recollimating the illumination beam and the lens refocusing the illumination beam through the pinhole. For simplicity, these imaging optics are designed to afocally and telecentrically image the plane $z = 0$ in V to the plane of the pinhole. The propagation of the field through the exit imaging optics can then be described by a space-invariant point-spread function $P(\mathbf{r}'';k) = (2\pi)^{-2}\int \mathrm{d}^2 q''\exp(-i\mathbf{q}''\cdot\mathbf{r}'')\tilde{P}(\mathbf{q}''/k)$, where the angular spectrum $\tilde{P}(\mathbf{q}''/k)$ is the coherent transfer function of the exit optics. The total Green's function $g(\mathbf{r},\mathbf{r}';k)$ that describes the propagation to the pinhole plane is

$$g(\mathbf{r},\mathbf{r}';k) = \frac{ik}{2\pi}\int_{z''=0} \mathrm{d}^2 r''\, P(\mathbf{r}-\mathbf{r}'';k) \int \mathrm{d}^2 q\, k_z(\mathbf{q})^{-1} \times \exp[i(\mathbf{q}\cdot(\mathbf{r}''-\mathbf{r}') + k_z(\mathbf{q})(z''-z'))], \tag{4}$$

using the Weyl expansion of a spherical wave as plane waves. This can be simplified by inserting the definition of $P(\mathbf{r};k)$:

$$g(\mathbf{r},\mathbf{r}';k) = ik(2\pi)^{-3}\int_{z''=0} \mathrm{d}^2 r'' \int \mathrm{d}^2 q''\exp[-i\mathbf{q}''\cdot(\mathbf{r}-\mathbf{r}'')] \times \tilde{P}\left(\frac{\mathbf{q}''}{k}\right)\int \mathrm{d}^2 q\, k_z(\mathbf{q})^{-1}\exp[i(\mathbf{q}\cdot(\mathbf{r}''-\mathbf{r}') + k_z(\mathbf{q})(z''-z'))]. \tag{5}$$

Switching the order of the integrations, the integration over $\mathbf{r}''$ yields $(2\pi)^2\delta^{(2)}(\mathbf{q}''+\mathbf{q})$. Further integration over $\mathbf{q}''$ yields

$$g(\mathbf{r},\mathbf{r}';k) = \frac{ik}{2\pi}\int \mathrm{d}^2 q\, k_z(\mathbf{q})^{-1}\tilde{P}\left(-\frac{\mathbf{q}}{k}\right)\exp[i(\mathbf{q}\cdot(\mathbf{r}-\mathbf{r}') - k_z(\mathbf{q})z')]. \tag{6}$$

Next, the complex phase of the scattered field at the pinhole plane is determined. Substituting Eqs. (3) and (6) into Eq. (2) yields

$$u_0(\mathbf{r};k)\phi(\mathbf{r},\mathbf{r_0};k) = -2ik(2\pi)^{-3}\int_V \mathrm{d}^3 r'\, n_0(\mathbf{r}')n(\mathbf{r}'-\mathbf{r_0}) \times \int \mathrm{d}^2 q'\exp[i(\mathbf{q}'\cdot\mathbf{r}' + k_z(\mathbf{q}')z')]\tilde{B}\left(\frac{\mathbf{q}'}{k}\right) \times \int \mathrm{d}^2 q\, k_z(\mathbf{q})^{-1}\tilde{P}(-\mathbf{q}/k) \times \exp[i(\mathbf{q}\cdot(\mathbf{r}-\mathbf{r}') - k_z(\mathbf{q})z')]. \tag{7}$$

The pinhole is placed so its center is at position $\mathbf{r} = \mathbf{0}$ on the pinhole plane. We assume that the pinhole is small enough that the value of $\phi(\mathbf{r},\mathbf{r_0};k)$ at $\mathbf{r} = \mathbf{0}$ is similar to its value over the entire pinhole. In this case, we concern

ourselves only with the value $\phi(\mathbf{0},\mathbf{r_0};k)$. We define the Fourier transform $\tilde{\phi}(\mathbf{Q};k)=\int d^3r_0 \exp(i\mathbf{Q}\cdot\mathbf{r_0})\phi(\mathbf{0},\mathbf{r_0};k)$, and substitute it into Eq. (7):

$$u_0(\mathbf{0};k)\tilde{\phi}(\mathbf{Q};k) = -2ik(2\pi)^{-3}\int d^3r_0\int_V d^3r'\, n_0(\mathbf{r}')n(\mathbf{r}'-\mathbf{r_0}) \times\exp(i\mathbf{Q}\cdot\mathbf{r_0})\int d^2q'\exp[i(\mathbf{q}'\cdot\mathbf{r}' + k_z(\mathbf{q}')z')]\tilde{B}\left(\frac{\mathbf{q}'}{k}\right)\int d^2q\, k_z(\mathbf{q})^{-1}\tilde{P}\left(-\frac{\mathbf{q}}{k}\right) \times\exp[i(-\mathbf{q}\cdot\mathbf{r}' - k_z(\mathbf{q})z')]. \quad (8)$$

Switching the order of integration and performing the integral over $\mathbf{r_0}$, we can identify the Fourier transform of $n(\mathbf{r})$:

$$u_0(\mathbf{0};k)\tilde{\phi}(\mathbf{Q};k) = -2ik(2\pi)^{-3}\tilde{n}(\mathbf{Q})\int d^2q'\,\tilde{B}\left(\frac{\mathbf{q}'}{k}\right) \times\int d^2q\, k_z(\mathbf{q})^{-1}\tilde{P}\left(-\frac{\mathbf{q}}{k}\right)\int_V d^2r'_\parallel dz' n_0(\mathbf{r}') \times\exp[i(\mathbf{Q}_\parallel\cdot\mathbf{r}'_\parallel + Q_z z')]\exp[i(\mathbf{q}'\cdot\mathbf{r}'_\parallel + k_z(\mathbf{q}')z')]\exp[i(-\mathbf{q}\cdot\mathbf{r}'_\parallel - k_z(\mathbf{q})z')], \quad (9)$$

where $z'=\mathbf{r}'\cdot\hat{\mathbf{z}}$, $\mathbf{r}'_\parallel=\mathbf{r}'-z'\hat{\mathbf{z}}$, $Q_z=\mathbf{Q}\cdot\hat{\mathbf{z}}$ and $\mathbf{Q}_\parallel=\mathbf{Q}-\hat{\mathbf{z}}Q_z$. In the volume V, without an object, the refractive index is a constant value n_b, so that $n_0(\mathbf{r}')=n_b$ in V. The integral over $\mathbf{r}'_\parallel$ can then be integrated to be a two-dimensional delta function:

$$u_0(\mathbf{0};k)\tilde{\phi}(\mathbf{Q};k) = -2ikn_b(2\pi)^{-1}\tilde{n}(\mathbf{Q})\int d^2q'\,\tilde{B}\left(\frac{\mathbf{q}'}{k}\right) \times\int d^2q\, k_z(\mathbf{q})^{-1}\tilde{P}\left(-\frac{\mathbf{q}}{k}\right)\int_V dz' \times\delta^{(2)}(\mathbf{Q}_\parallel+\mathbf{q}'-\mathbf{q})\exp(iQ_z z') \times\exp[ik_z(\mathbf{q}')z']\exp[-ik_z(\mathbf{q})z']. \quad (10)$$

Performing the integration over $\mathbf{q}'$ yields

$$u_0(\mathbf{0};k)\tilde{\phi}(\mathbf{Q};k) = -2ikn_b(2\pi)^{-1}\tilde{n}(\mathbf{Q})\int d^2q\, k_z(\mathbf{q})^{-1} \times\tilde{P}\left(-\frac{\mathbf{q}}{k}\right)\tilde{B}\left(\frac{\mathbf{q}-\mathbf{Q}_\parallel}{k}\right)\int_V dz'\exp(iQ_z z') \times\exp[ik_z(\mathbf{q}-\mathbf{Q}_\parallel)z']\exp[-ik_z(\mathbf{q})z']. \quad (11)$$

Performing the integration over z' yields a one-dimensional delta function:

$$u_0(\mathbf{0};k)\tilde{\phi}(\mathbf{Q};k) = -2ikn_b\tilde{n}(\mathbf{Q})\int d^2q\, k_z(\mathbf{q})^{-1}\tilde{P}\left(-\frac{\mathbf{q}}{k}\right) \times\tilde{B}\left(\frac{\mathbf{q}-\mathbf{Q}_\parallel}{k}\right)\delta[Q_z + k_z(\mathbf{q}-\mathbf{Q}_\parallel) - k_z(\mathbf{q})]. \quad (12)$$

For brevity, one can define a 3-D transfer function of the instrument by

$$\tilde{F}(\mathbf{Q};k) = -2in_b\int d^2q\, k_z(\mathbf{q})^{-1}\tilde{P}\left(-\frac{\mathbf{q}}{k}\right)\tilde{B}\left(\frac{\mathbf{q}-\mathbf{Q}_\parallel}{k}\right) \times\delta[Q_z + k_z(\mathbf{q}-\mathbf{Q}_\parallel) - k_z(\mathbf{q})] \quad (13)$$

so that $u_0(\mathbf{0};k)\tilde{\phi}(\mathbf{Q};k)=k\tilde{n}(\mathbf{Q})\tilde{F}(\mathbf{Q};k)$.

The complex phase ϕ is then the 3-D convolution of the index profile $n(\mathbf{r})$ and a 3-D point-spread function. For a version of Eq. (13) suitable for numerical integration, see Appendix A. However, ϕ cannot be measured directly. Rather, we measure the intensity at the pinhole of the interference between the reference and sample signals and infer the sample field at the pinhole, and from this the complex phase. Given the definition of the complex phase, the sample field at the pinhole will be $u_s = u_0(\mathbf{0};k)\exp[\phi(\mathbf{0},\mathbf{r_0};k)]$. The reference field at the pinhole is delayed by a time τ relative to the sample field, so that the field is given by $u_r\exp(ikc\tau)$, where c is the speed of light. The total field at the pinhole is

$$I(\mathbf{r_0};k,\tau) = |u_r\exp(ikc\tau) + u_0(\mathbf{0};k)\exp[\phi(\mathbf{0},\mathbf{r_0};k)]|^2. \quad (14)$$

By performing phase shifting and measuring $I(\mathbf{r_0};k,\tau)$ for three values of τ such that $kc\tau=0$, $\pi/2$, and π, the complex phase can be found:

$$\phi(\mathbf{0},\mathbf{r_0};k) = \log\left\{[u_r^* u_0(\mathbf{0};k)]^{-1}\left[\frac{1-i}{4}I(\mathbf{r_0};k,0) - \frac{1+i}{4}I(\mathbf{r_0};k,\pi/ck) + \frac{i}{2}I(\mathbf{r_0};k,\pi/2ck)\right]\right\}. \quad (15)$$

The log in Eq. (15) is the complex logarithm, which is multiple valued so there is an ambiguity of a multiple of $2\pi i$. Because of this ambiguity, phase unwrapping needs to be performed on $\phi(\mathbf{0},\mathbf{r_0};k)$. This can be problematic if there are values of $\mathrm{Re}\{\phi(\mathbf{0},\mathbf{r_0};k)\}$ that are well below zero, so that the phase is poorly estimated at these points.

3. GROUP REFRACTIVE INDEX MEASUREMENT

In practice, the imaginary part of ϕ may be difficult to measure because it depends sensitively on changes of the total optical path length through the interferometer on the order of a wavelength. Rather, one can use the phase difference between different illumination frequencies to estimate the group refractive index. Upon differentiation of $u_0\tilde{\phi}$ with respect to k, we find

$$\frac{\mathrm{d}(u_0\tilde{\phi})}{\mathrm{d}k} = \tilde{n}\tilde{F} + k\frac{\mathrm{d}\tilde{n}}{\mathrm{d}k}\tilde{F} + k\tilde{n}\frac{\mathrm{d}\tilde{F}}{\mathrm{d}k}. \tag{16}$$

We now assume that $\mathrm{d}\tilde{F}/\mathrm{d}k$ has little wavelength dependence, so that $\mathrm{d}\tilde{F}/\mathrm{d}k \approx 0$. The function $\tilde{F}$ is dependent on the beam spectrum $\tilde{B}$ and the aperture spectrum $\tilde{P}$. The definitions of the aperture functions $\tilde{B}$ and $\tilde{P}$ are achromatic for the purpose of minimizing $|\mathrm{d}\tilde{F}/\mathrm{d}k|$. For focused beams where all frequencies have the same NA, the primary difference between the beams is the spot sizes at the focus, which scale with k^{-1}. For a small fractional bandwidth of illumination (e.g., 10%–20%) the contribution due to $\mathrm{d}\tilde{F}/\mathrm{d}k$ will be small. Neglecting $\mathrm{d}\tilde{F}/\mathrm{d}k$ it is found that

$$\frac{\mathrm{d}(u_0\tilde{\phi})}{\mathrm{d}k} = \tilde{F}(\mathbf{Q};k)\left[\tilde{n} + k\frac{\mathrm{d}\tilde{n}}{\mathrm{d}k}\right] = \tilde{F}(\mathbf{Q};k)\tilde{n}_g(\mathbf{Q}). \tag{17}$$

In Eq. (17), the group refractive index is the term $\tilde{n}_g = \tilde{n} + k(\mathrm{d}\tilde{n}/\mathrm{d}k)$. This indicates that $\mathrm{d}(u_0\phi)/\mathrm{d}k$ is the 3-D convolution of the group refractive index of the object with the 3-D point-spread function of the beam. Therefore, deconvolution of $\mathrm{d}(u_0\phi)/\mathrm{d}k$ can be used to estimate the 3-D distribution of the group refractive index of the object. Because $\mathrm{d}(u_0\phi)/\mathrm{d}k$ is made with a differential measurement between samples of ϕ at two or more frequencies k, it does not depend on the absolute phase delay through the object and therefore is easier to measure. The imaginary part of $\mathrm{d}\phi/\mathrm{d}k$ is the differential group optical path length between the reference and sample arms.

To measure the frequency-dependent complex phase, one can use a spectrometer (such as a grating spectrometer) that measures the spectrum of the signal passing through the pinhole. Spectral interferometry enables the interferometric cross correlation of the reference and sample beams to be inferred from the measured spectrum. The intensity measured at a particular frequency in the spectrometer [indicated in Eq. (14)] can be divided into three components: the spectrum of the reference alone, the spectrum of the signal passing through the sample alone, and the interference component between the reference and object signals:

$$I(\mathbf{r_0};k,\tau) = |u_r|^2 + |u_0(\mathbf{0};k)\exp[\phi(\mathbf{0},\mathbf{r_0};k)]|^2 + 2\,\mathrm{Re}\{u_r^* u_0(\mathbf{0};k)\exp[\phi(\mathbf{0},\mathbf{r_0};k) - ikc\tau]\}. \tag{18}$$

Phase shifting can be used to distinguish the interference component. Alternatively, if the reference signal precedes the sample signal sufficiently in time that the two do not overlap, the Hilbert transform can be used to compute the complex analytic signal of the interferogram, which contains the phase and amplitude of $u_r^* u_0(\mathbf{0};k)$.

Again, the field scattered by the object is $u_s(\mathbf{0},\mathbf{r_0};k) = u_0(\mathbf{0};k)\exp[\phi(\mathbf{0},\mathbf{r_0};k)]$. To compute ϕ from this, the logarithm function must be used, so again there is a phase ambiguity of 2π. Fortunately, the phase-wrapping problem can be avoided because $\mathrm{d}(u_0\phi)/\mathrm{d}k$ is needed to measure the group refractive index, not ϕ itself. For brevity, define $u_0\phi' = \mathrm{d}(u_0\phi)/\mathrm{d}k$, which is given by

$$u_0\phi' = \frac{\mathrm{d}(u_0\phi)}{\mathrm{d}k} = u_0\frac{\mathrm{d}\phi}{\mathrm{d}k} + \frac{\mathrm{d}u_0}{\mathrm{d}k}\phi. \tag{19}$$

To simplify Eq. (19), we now examine Eq. (3) with the condition $\mathbf{r}' = \mathbf{0}$, the position of the pinhole. As defined, the amplitudes of all of beams at frequencies k are the same at their respective foci. Because the exit imaging optics are achromatic, the same will be true at the pinhole. Therefore $\mathrm{d}u_0/\mathrm{d}k = 0$ and $\phi' = \mathrm{d}\phi/\mathrm{d}k$. Using this fact, a finite-difference approximation from two samples of the field u_s at frequencies k and $k+\Delta k$ can be found:

$$\begin{aligned}\phi' = \frac{\mathrm{d}\phi}{\mathrm{d}k} &\approx \frac{\phi(\mathbf{0},\mathbf{r_0};k+\Delta k) - \phi(\mathbf{0},\mathbf{r_0};k)}{\Delta k} \\ &= \frac{\log\dfrac{u_s(\mathbf{0},\mathbf{r_0};k+\Delta k)}{u_0(\mathbf{0};k+\Delta k)} - \log\dfrac{u_s(\mathbf{0},\mathbf{r_0};k)}{u_0(\mathbf{0};k)}}{\Delta k} \\ &= \frac{1}{\Delta k}\log\frac{u_s(\mathbf{0},\mathbf{r_0};k+\Delta k)}{u_s(\mathbf{0},\mathbf{r_0};k)}\frac{u_0(\mathbf{0};k)}{u_0(\mathbf{0};k+\Delta k)} \\ &= \frac{1}{\Delta k}\log\frac{u_s(\mathbf{0},\mathbf{r_0};k+\Delta k)}{u_s(\mathbf{0},\mathbf{r_0};k)}.\end{aligned} \tag{20}$$

If instead of sampling u_s at just two frequencies, the field u_s is sampled at N frequencies k_i where $1 \le i \le N$, as would occur for a spectrometer sampling an entire interferometric spectrum. An estimate of the average ϕ' over the interval k_1 to k_N can be calculated using

$$\phi' = \sum_{i=1}^{N-1}\frac{1}{k_{i+1}-k_i}\log\frac{u_s(\mathbf{0},\mathbf{r_0};k_{i+1})}{u_s(\mathbf{0},\mathbf{r_0};k_i)}. \tag{21}$$

Because the phases between the samples of u_s are subtracted by the division operation before the logarithm is taken, phase wrapping is not necessary to compute ϕ'. The complex logarithm need only be applied on the principal branch with imaginary part between $-i\pi$ and $i\pi$. Limiting the logarithm to this branch effectively requires that the phase differences between adjacent samples of u_s be less than π and greater than $-\pi$.

Because a spectrometer can capture the data needed to compute an estimate of ϕ' without requiring phase shifting or phase unwrapping, we believe this method is a potentially robust and sensitive way to measure the group refractive index of a sample with diffraction-limited resolution in three dimensions. The sample must simply be translated in three dimensions while the spectrum of the field at the pinhole is sampled. Using the Hilbert transform to infer the phase of the interferogram avoids phase shifting, and the fact that only phase differences are needed avoids the phase-unwrapping requirement, which simplifies the apparatus and minimizes error.

4. LINEAR SOLUTIONS TO THE INVERSE PROBLEM FOR GROUP REFRACTIVE INDEX

Equation (17) expresses the relationship between the group refractive index of an object and the complex phase of a beam passing through the object. In the spatial do-

main, this relationship is a 3-D convolution of the group refractive index with a point-spread function:

$$u_0\boldsymbol{\phi}' = u_0(\mathbf{0};k)\phi'(\mathbf{r_0};k) = \mathbf{F}\mathbf{n_g} = \int_V \mathrm{d}^3r\, n_g(\mathbf{r})F(\mathbf{r_0}-\mathbf{r};k),$$

$$\text{with } F(\mathbf{r};k) = (2\pi)^{-3}\int \mathrm{d}^3Q\, \exp(-i\mathbf{r}\cdot\mathbf{Q})\tilde{F}(\mathbf{Q};k),$$

$$n_g(\mathbf{r}) = (2\pi)^{-3}\int \mathrm{d}^3Q\, \exp(-i\mathbf{r}\cdot\mathbf{Q})\tilde{n}_g(\mathbf{Q}). \tag{22}$$

The operator equation $u_0\boldsymbol{\phi}' = \mathbf{F}\mathbf{n_g}$ implicitly defines the operator $\mathbf{F}$ in terms of the 3-D convolution of the kernel $F(\mathbf{r};k)$ with the refractive index function $n_g(\mathbf{r})$ as shown in Eq. (22). With this specification of the forward problem, we can pose the inverse problem as the minimization of a squared error functional:

$$\begin{aligned} n_g^+ &= \arg\min_{n_g} |u_0\boldsymbol{\phi}' - \mathbf{F}\mathbf{n_g}|^2 + \gamma|\mathbf{n_g}|^2 \\ &= \arg\min_{n_g} \int_V \mathrm{d}^3r_0 |u_0(\mathbf{0};k)\phi'(\mathbf{r_0};k) \\ &\quad - \int_V \mathrm{d}^3r\, n_g(\mathbf{r})F(\mathbf{r_0}-\mathbf{r};k)|^2 + \gamma\int_V \mathrm{d}^3r|n_g(\mathbf{r})|^2. \end{aligned} \tag{23}$$

The term proportional to γ is included to effect Tikhonov regularization to stabilize the solution. Formally, the solution is given by the Tikhonov-regularized pseudoinverse solution $\mathbf{n_g^+} = (\mathbf{F}^\dagger\mathbf{F} + \gamma\mathbf{I})^{-1}\mathbf{F}^\dagger u_0\boldsymbol{\phi}'$. Because the operation of $\mathbf{F}$ on a function $u_0\phi'$ is a 3-D convolution, it is easier to express the pseudoinverse in the frequency domain:

$$\tilde{n}_g^+(\mathbf{Q};k) = \frac{u_0(\mathbf{0};k)\tilde{\phi}'(\mathbf{Q};k)\tilde{F}^*(\mathbf{Q};k)}{|\tilde{F}(\mathbf{Q};k)|^2 + \gamma}. \tag{24}$$

However, the space-invariant filter of Eq. (24), while simple to implement, suffers from a deficiency. Because the calculated phase difference ϕ' is given by a logarithmic relationship to u_s by Eq. (20), a constant error variance in the measurement of u_s does not necessarily produce a constant error variance in ϕ'. Given the differential relation $\phi' = (\mathrm{d}u_s/\mathrm{d}k)/u_s$, it is clear that smaller $|u_s|$ will produce a larger error in ϕ'. It is desirable to modify the solution to account for the error in individual measurements of ϕ'. We define an alternate least-squares minimization that weights the error according to the confidence in various samples of ϕ':

$$\begin{aligned} n_g^+ &= \arg\min_{n_g} |\mathbf{W}(u_0\phi' - \mathbf{F}\mathbf{n_g})|^2 + \gamma|\mathbf{n_g}|^2 \\ &= \arg\min_{n_g} \int_V \mathrm{d}^3r_0 |W(\mathbf{r_0})|^2 \Bigg| u_0(\mathbf{0};k)\phi'(\mathbf{0},\mathbf{r_0};k) \\ &\quad - \int_V \mathrm{d}^3r\, n_g(\mathbf{r})F(\mathbf{r_0}-\mathbf{r};k)\Bigg|^2 + \gamma\int_V \mathrm{d}^3r|n_g(\mathbf{r})|^2. \end{aligned} \tag{25}$$

This expression defines a weighting operator $\mathbf{W}$ in the spatial domain V with a corresponding weighting function $W(\mathbf{r_0})$, which is assigned greater weights to values of $\phi'(\mathbf{0},\mathbf{r_0};k)$ for which there is greater certainty. The weighting function that properly accounts for the confidence in ϕ' given a constant error variance for u_s is $W(\mathbf{r_0}) = \exp[\mathrm{Re}\,\phi(\mathbf{0},\mathbf{r_0};k)]$. The weighted, Tikhonov-regularized formal solution is $\mathbf{n_g^+} = (\mathbf{F}^\dagger\mathbf{W}^\dagger\mathbf{W}\mathbf{F} + \gamma\mathbf{I})^{-1}\mathbf{F}^\dagger\mathbf{W}^\dagger\mathbf{W}u_0\boldsymbol{\phi}'$. Because of the weighting in the spatial domain, the solution can no longer be computed using a space-invariant filter. However, the operators $\mathbf{W}$ and $\mathbf{F}$ are diagonal in their respective domains, so the numerical solution of the problem lends itself well to sparse matrix methods such as the preconditioned conjugate-gradient method [21].

5. SIMULATION AND DISCUSSION

To show the feasibility of measuring group refractive index with the proposed method, a simulation was performed to demonstrate the resolution and noise resilience of the method. The simulated object is a refracting and absorbing spherical shell with spherical inclusions intended to be a simple phantom evocative of cells with their constituent organelles. The simulated volume is $75\lambda \times 75\lambda \times 75\lambda$ in size sampled every $\lambda/2$, where λ is the center wavelength of the illumination. The shell is 35λ in diameter and 3λ thick. The background refractive index is 1.0, and all of the refractive indices of the simulation scale with this index (e.g., if the background index were 1.33, all of the reconstructed indices would likewise be multiplied by 1.33). The inclusions are also spheres 3λ in diameter. The shell has a refractive index of $1.2+0.02i$, and the inclusions have a refractive index of $1.06+0.02i$. Figures 2(a) and 2(b) detail a slice through the synthetic object, showing the real and imaginary parts of the refractive index of the object.

The simulated optical system has two NAs associated with it: the NA of the illumination beam optics and the NA of the relay optics to the pinhole. In our simulation, they were both set to have NA of 0.75. The functions $\tilde{B}(\mathbf{q}/k) = 1$ and $\tilde{P}(\mathbf{q}/k) = 1$ for $|\mathbf{q}| < (NA)k$ and zero otherwise. Using these functions, the 3-D transfer function $\tilde{F}(\mathbf{Q};k)$ was calculated using Eq. (28) and numerical integration. A 2-D projection of the 3-D function $|\tilde{F}(\mathbf{Q};k)|$ is shown in Fig. 3(a), which shows the bandpass of the optical system in terms of the transverse and axial spatial frequencies as a fraction of k, the illumination wavenumber. Because this simulation is of scalar fields, the 3-D point frequency response is rotationally symmetric about $|\mathbf{Q}_\parallel| = 0$. The 2-D projection of the 3-D point-spread function, which is the inverse 3-D Fourier transform of $\tilde{F}(\mathbf{Q};k)$, is shown in Fig. 3(b). This shows the axial and transverse resolution of the system in units of λ and is likewise rotationally symmetric.

Using the phantom and the calculated frequency response of the system, the synthetic interferometric data were computed. To do this, first the complex phase $\phi(\mathbf{0},\mathbf{r_0};k)$ was calculated at frequencies k and $k+\Delta k$ using the 3-D convolution of the refractive index profile with the 3-D impulse response as in Eq. (13). In the simulation, $\Delta k = 0.03k$, so that the group delay is being measured

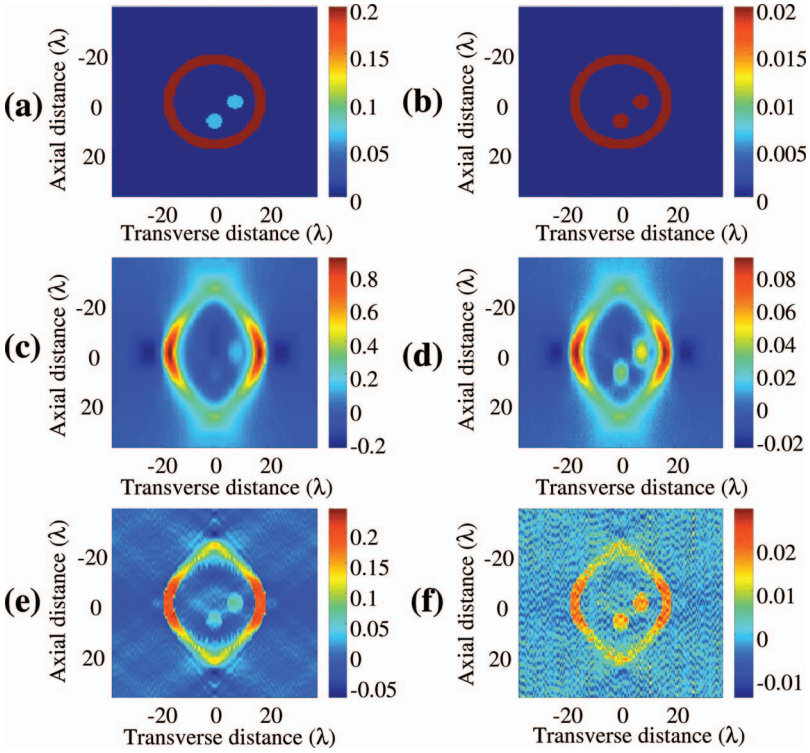

Fig. 2. (a), (b), Images of the same slice through the center plane of the simulated phantom: (a) real part of the refractive index, (b) imaginary part. (c), (d), Images of the data acquired by the confocal instrument of these planes: (c) total number of radians of retardance between the two measured frequencies recorded at each beam position, (d) total attenuation difference in nats between the two measured frequencies recorded at each beam position. (e) Real part of the weighted least-squares reconstruction of the index profile, (f) imaginary part.

from a 3% fractional bandwidth. The field $u_s = u_0(\mathbf{0};k)\exp[\phi(\mathbf{0},\mathbf{r_0};k)]$ was calculated at the two frequencies, and from this the intensity of the interferometric measurements $I(\mathbf{r_0};k,\tau)$ could be calculated using Eq. (18) for $\tau = 0, \pi/2$, and π. Noise was added to the measured intensity to achieve a signal-to-noise ratio (SNR) of 20 dB. The synthetic data $\phi'\Delta k$ is detailed in Figs. 2(c) and 2(d), which are the difference in retardance (c) and attenuation (d) between the frequencies k and $k+\Delta k$ measured at each position of the illumination beam. The total retardance difference between the two frequencies in Fig. 2(c) is given in radians and corresponds to the real part of $\phi'\Delta k$. The total attenuation difference between the two frequencies in Fig. 2(d) is given in nats (also called nepers) and corresponds to the imaginary part of $\phi'\Delta k$.

Using the synthetic data, which consisted of interferometric intensity samples measured at two frequencies k and $k+\Delta k$ and three different τ over $\mathbf{r_0}$, the inverse scattering process was performed as follows:

1. From the intensity samples, estimates of ϕ were computed with Eq. (15).
2. From ϕ, estimates of u_s were computed using $u_s = u_0 \exp \phi$.
3. With ϕ and u_s, an estimate of ϕ' was calculated with Eq. (20).
4. The weighting function was calculated using $W(\mathbf{r_0}) = \exp[\mathrm{Re}\,\phi(\mathbf{0},\mathbf{r_0};k)]$, which assigns larger weights to estimates of ϕ' for which more power from the sample arm was detected at the pinhole.

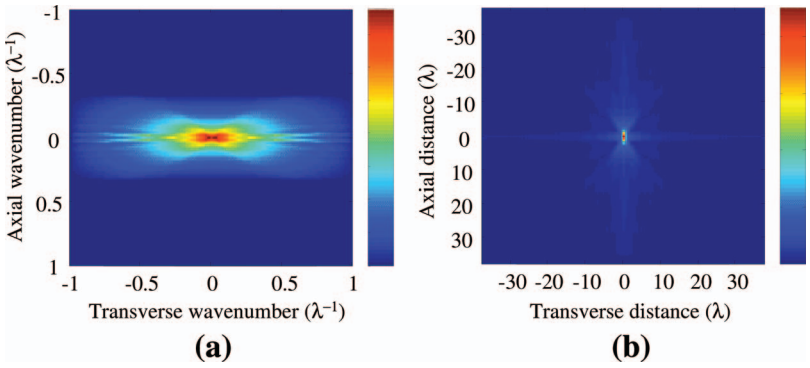

Fig. 3. (a) 2-D projection along one transverse axis of the 3-D transfer function $\tilde{F}(\mathbf{Q};k)$ of the simulated confocal microscope. The function is radially symmetric about the $Q_{\|}=0$ axis. (b) 2-D projection along one transverse axis of the 3-D point-spread function of the simulated confocal microscope. The point-spread function is likewise radially symmetric. Both density plots use relative units.

5. The weighted least-squares solution of Eq. (25) for n_g^+ was computed using the preconditioned conjugate-gradient method. The system solved was formally $(\mathbf{F}^\dagger\mathbf{W}^\dagger\mathbf{W}\mathbf{F}+\gamma\mathbf{I})\mathbf{n}_\mathbf{g}^+=\mathbf{F}^\dagger\mathbf{W}^\dagger\mathbf{W}u_0\boldsymbol{\phi}'$. The preconditioner was the unweighted inverse solution, given by the space-invariant operator $(\mathbf{F}^\dagger\mathbf{F}+\gamma\mathbf{I})^{-1}$.

The result of the inversion is shown in the refractive index reconstruction of Figs. 2(e) and 2(f). Figure 2(e) corresponds to the reconstructed real part of the refractive index, and Fig. 2(f) corresponds to the imaginary part. Because of the finite NA and frequency space coverage of the instrument, it is clear that the reconstructed object has been elongated in the axial direction. This elongation is consistent with the depth of field of a typical microscope with the simulated NA. On the boundaries of the outer sphere parallel to the axial direction, there is less elongation and the estimate of the refractive index is more accurate. In addition, the estimated refractive index of the inclusions is also elongated, but it remains similar to the phantom. While the simulation does not show a perfectly reconstructed object, it depicts the limitations that an actual instrument would have because the object is illuminated with a finite-NA beam from a single direction.

A rough estimate of the magnitude of the noise in the refractive index reconstruction can be computed. In general, the refractive index variation Δn will depend on the NA, the fractional bandwidth of the source $\Delta k/k$, and the SNR of the measurements. Tighter focusing will provide better resolution, but less retardation is produced at the focus as the depth of focus is decreased. More bandwidth will produce a larger difference in retardance at the extremes of the source spectrum. Finally, higher SNR allows one to better distinguish small phase variations, with the minimum detectable phase difference being approximately $(SNR)^{-1}$ in radians [22,23] (SNR being defined in this work on the fields). Accounting for these factors, we estimate that $\Delta n=[n_b k(NA)^2]/[2\pi\Delta k(SNR)]$. For the simulation, $\Delta n\approx 0.03$, which is consistent with the noise seen in Figs. 2(e) and 2(f).

In addition, the simulation shows that if the illumination is limited to one direction, unavoidable blurring in the axial direction can be expected. This is a limitation of any confocal microscope, and it can be mitigated by imaging the object from multiple illumination angles rather than fixing the orientation of the illumination beam relative to the object. In practice, axial resolution on the order of a few wavelengths (for near-infrared or visible light) provides μm-scale resolution, which is adequate for many applications.

In conclusion, we have proposed and simulated a novel microscope to measure group refractive index. The instrument will allow the microscopic variations of tissue refractive index to be investigated. The robustness of the instrument derives from the fact that it requires only relative phase and amplitude measurements between two or more wavelengths transmitted through the object. Relative measurements are less error prone than absolute measurements of the total phase retardance and attenuation, especially because the interference measurements at different frequencies can be captured simultaneously with an array spectrometer. For this reason we believe the proposed instrument will make a fundamental material optical property, group refractive index, more accessible.

APPENDIX A

Equation (13) for $\tilde{F}(\mathbf{Q};k)$ is a two-dimensional integral with a one-dimensional delta function, which we simplify into a one-dimensional integral. We change variables to $\mathbf{s}=\mathbf{Q}_\parallel/2-\mathbf{q}$, define $\cos\theta=(\mathbf{Q}_\parallel\cdot\mathbf{s})/Q_\parallel s$, and rewrite the integral as

$$\tilde{F}(\mathbf{Q};k)=-2in_b\int_{-\pi/2}^{\pi/2}\mathrm{d}\theta\int_0^\infty \mathrm{d}s\, sk_z(\mathbf{q})^{-1}\tilde{P}\left(-\frac{\mathbf{q}}{k}\right)\times\tilde{B}\left(\frac{\mathbf{q}-\mathbf{Q}_\parallel}{k}\right)\delta[f(s)],$$

$$\text{with } f(s)=Q_z+\sqrt{k^2-\left(\frac{Q_\parallel}{2}\right)^2-s^2-Q_\parallel s\cos\theta}-\sqrt{k^2-\left(\frac{Q_\parallel}{2}\right)^2-s^2+Q_\parallel s\cos\theta}. \tag{26}$$

In the inner integral, the delta function selects the values such that $f(s)=0$, which are

$$s=\pm\frac{Q_z\sqrt{4k^2-Q_\parallel^2-Q_z^2}}{2\sqrt{Q_z^2+Q_\parallel^2\cos^2\theta}}. \tag{27}$$

Because the integration bounds on s are for nonnegative s, only the positive root need be considered. Using the sifting theorem, Eq. (26) integrates to

$$\tilde{F}(\mathbf{Q};k)=-2in_b\int_{-\pi/2}^{\pi/2}\mathrm{d}\theta\, sk_z(\mathbf{q})^{-1}\tilde{P}\left(-\frac{\mathbf{q}}{k}\right)\tilde{B}\left(\frac{\mathbf{q}-\mathbf{Q}_\parallel}{k}\right)\times\left|\frac{\mathrm{d}f}{\mathrm{d}s}\right|^{-1},$$

$$\text{with } s=\frac{|Q_z|\sqrt{4k^2-Q_\parallel^2-Q_z^2}}{2\sqrt{Q_z^2+Q_\parallel^2\cos^2\theta}},$$

$$\mathbf{q}=\frac{\mathbf{Q}_\parallel}{2}-\frac{\mathbf{Q}_\parallel}{Q_\parallel}s\cos\theta-\frac{\mathbf{Q}_\perp}{Q_\perp}s\sin\theta,\quad \mathbf{Q}_\perp\cdot\{\mathbf{Q}_\parallel,\hat{\mathbf{z}}\}=0,$$

$$\frac{\mathrm{d}f}{\mathrm{d}s}=\frac{2s-Q_\parallel\cos\theta}{2\sqrt{k^2-\left(\frac{Q_\parallel}{2}\right)^2-s^2+Q_\parallel s\cos\theta}}-\frac{2s+Q_\parallel\cos\theta}{2\sqrt{k^2-\left(\frac{Q_\parallel}{2}\right)^2-s^2-Q_\parallel s\cos\theta}}. \tag{28}$$

This formula can be numerically integrated to calculate $\tilde{F}(\mathbf{Q};k)$.

ACKNOWLEDGMENTS

We thank P. Scott Carney from the Beckman Institute for Advanced Science and Technology at the University of Illinois at Urbana-Champaign for his theoretical insight and review of this paper. This work was supported in part by grants to S. A. Boppart by the National Science Foundation (BES 03-47747, BES 06-19257) and the National Institutes of Health (Roadmap Initiative, NIBIB, 1 R21 EB005321). Additional information can be found at http://biophotonics.uiuc.edu.

REFERENCES

1. A. M. Zysk, E. J. Chaney, and S. A. Boppart, "Refractive index of carcinogen-induced rat mammary tumours," Phys. Med. Biol. **51**, 2165–2177 (2006).
2. L. Lepetit, G. Cheriaux, and M. Joffre, "Linear techniques of phase measurement by femtosecond spectral interferometry for applications in spectroscopy," J. Opt. Soc. Am. B **12**, 2467–2474 (1995).
3. S. Singh, "Refractive index measurement and its applications," Phys. Scr. **65**, 167–180 (2002).
4. A. M. Zysk, F. T. Nguyen, A. L. Oldenburg, D. L. Marks, and S. A. Boppart, "Optical coherence tomography: a review of clinical development from bench to bedside," J. Biomed. Opt. **12**, 051403 (2007).
5. S. R. Arridge, "Optical tomography in medical imaging," Inverse Probl. **15**, R41–R93 (1999).
6. Y.-P. Wang, D.-N. Wang, W. Jin, J.-P. Chen, X.-W. Li, and J.-H. Zhou, "Reflectometry measuring refractive index and thickness of polymer samples simultaneously," J. Mod. Opt. **53**, 1845–1851 (2006).
7. H. Takubo, "Refractive index as a measure for saturation and supersaturation in crystal growth of water-soluble substances," J. Cryst. Growth **104**, 239–244 (1990).
8. Z. Liu, X. Dong, Q. Chen, C. Yin, Y. Xu, and Y. Zheng, "Nondestructive measurement of an optical fiber refractive-index profile by a transmitted-light differential interference contact microscope," Appl. Opt. **43**, 1485–1492 (2004).
9. D. J. Faber, M. C. G. Aalders, E. G. Mik, B. A. Hooper, M. J. C. van Gemert, and T. G. van Leeuwen, "Oxygen saturation-dependent absorption and scattering of blood," Phys. Rev. Lett. **93**, 028102 (2004).
10. G. J. Tearney, M. E. Brezinski, J. F. Southern, B. E. Bouma, M. R. Hee, and J. G. Fujimoto, "Determination of the refractive index of highly scattering human tissue by optical coherence tomography," Opt. Lett. **20**, 2258–2260 (1995).
11. A. M. Zysk, J. J. Reynolds, D. L. Marks, P. S. Carney, and S. A. Boppart, "Projected index computed tomography," Opt. Lett. **28**, 701–703 (2003).
12. S. A. Alexandrov, A. V. Zvyagin, K. K. M. B. D. Silva, and D. D. Sampson, "Bifocal optical coherence refractometry of turbid media," Opt. Lett. **28**, 117–119 (2003).
13. A. V. Zvyagin, K. K. M. B. D. Silva, S. A. Alexandrov, T. R. Hillman, J. J. Armstrong, T. Tsuzuki, and D. D. Sampson, "Refractive index tomography of turbid media by bifocal optical coherence refractometry," Opt. Express **11**, 3503–3517 (2003).
14. W. Choi, C. Fang-Yen, K. Badizadegan, S. Oh, N. Lue, R. R. Dasari, and M. S. Feld, "Tomographic phase microscopy," Nat. Methods **4**, 717–719 (2007).
15. J. J. J. Dirckx, L. C. Kuypers, and W. F. Decraemer, "Refractive index of tissue measured with confocal microscopy," J. Biomed. Opt. **10**, 044014 (2005).
16. I. K. Ilev, R. W. Waynant, K. R. Byrnes, and J. J. Anders, "Dual confocal fiber-optic method for measurement of refractive index and thickness of optically transparent media," Opt. Lett. **27**, 1603–1605 (2002).
17. D. F. Aldridge, "Linearization of the eikonal equation," Geophysics **59**, 1631–1632 (1994).
18. R. Snieder and D. F. Aldridge, "Perturbation theory for travel times," J. Acoust. Soc. Am. **98**, 1565–1569 (1995).
19. M. Born and E. Wolf, *Principles of Optics* (Cambridge U. Press, 1980).
20. G. Gbur and E. Wolf, "Relation between computed tomography and diffraction tomography," J. Opt. Soc. Am. A **18**, 2132–2137 (2001).
21. G. H. Golub and C. F. Van Loan, *Matrix Computations* (Johns Hopkins U. Press, 1996).
22. J. Fingler, D. Schwartz, C. Yang, and S. E. Fraser, "Mobility and transverse flow visualization using phase variance contrast with spectral optical coherence tomography," Opt. Express **15**, 12636–12653 (2007).
23. B. H. Park, M. C. Pierce, B. Cense, S.-H. Yun, M. Mujat, G. J. Tearney, B. E. Bouma, and J. F. de Boer, "Real-time fiber-based multi-functional spectral-domain optical coherence tomography at 1.3 microns," Opt. Express **13**, 3931–3944 (2005).